JPSE (Journal of Physical Science and Engineering), Vol. 9, No. 2, 2024, Page 85–93.
DOI: 10.17977/um024v9i22024p85-93

JPSE
(Journal of Physical Science and Engineering)

http://journal2.um.ac.id/index.php/jpse
EISSN: 2541-2485

Comprehensive Investigation of MXene and Cassava Tubers-Bamboo Stems Activated Carbon Electrodes: Configuration-Dependent Supercapacitor Performances

Received
2 September 2024

Revised
30 September 2024

Accepted for Publication
2 October 2024

Published
31 October 2024

Nuviya Illa Muthi Aturroifah, Markus Diantoro*, Nasikhudin

1. Departement of Physics, Faculty of Mathematics and Natural Sciences, Universitas Negeri Malang, Jl. Semarang 5, Malang 65145, Indonesia.

*Corresponding Author's E-mail: markus.diantoro.fmipa@um.ac.id

Abstract

This study explores the structural, morphological, and electrochemical characteristics of supercapacitor active materials derived from MXene ($Ti_3C_2T_x$) and activated carbon (AC) synthesized from cassava tubers and bamboo stems. The etching process using HF effectively converted the MAX phase into MXene, confirmed by the disappearance of the (104) diffraction peak and the shift of the (002) peak to a lower diffraction angle, indicating increased interlayer spacing due to aluminum removal and intercalation of functional groups and water molecules. SEM analysis revealed that MXene exhibits thinner layered structures with reduced crystallite size (112.65-8.13 nm), confirming the formation of a highly conductive two-dimensional structure. Meanwhile, AC cassava tubers-bamboo stems presented an amorphous graphitic structure with a three-dimensional porous morphology resembling a sunflower pattern and an average pore diameter of 3.52 µm, which enhances ion transport and active surface area. Electrochemical performance evaluation demonstrated that the AC-MXene-Al Foil//AC-MXene-Cu Foil configuration achieved the highest performance, with a specific capacitance of 46.201 Fg^{-1}, energy density of 5.770 $Whkg^{-1}$, and power density of 18.996 Wkg^{-1}. Dunn method analysis revealed that the charge storage mechanism is primarily surface capacitive. These results demonstrate the promising potential of biomass-derived AC/MXene composites for high-performance and sustainable energy storage applications.

Keywords: Supercapacitor, MXene, Cassava Tubers-Bamboo Stems, Activated Carbon.

1. Introduction

Technological advancements have increased the demand for energy storage devices in various applications, including medical equipment, smartphones, microrobots, and other electronic systems [1]. Currently, batteries and supercapacitors are the most extensively developed energy storage technologies. Batteries offer several advantages, such as stable electricity delivery and high energy density. Batteries exhibit stable power output and high energy density but are limited by low power density and poor cycle stability. Supercapacitors offer several advantages over batteries, including higher power density (100–10,000 W kg^{-1}), longer cycle life (>100,000 cycles), rapid charging (≤2 minutes) and discharging (1–30 seconds) capabilities, and the use of more environmentally friendly [2]. Based on the electrode materials employed and the configuration between the cathode and anode, supercapacitors can be classified into symmetric and asymmetric types. Based on energy storage mechanisms, supercapacitors can be categorized into electric double-layer capacitors (EDLCs), pseudocapacitors, and hybrid supercapacitors. EDLCs and pseudocapacitors are symmetric supercapacitors in which the cathode and anode are composed of the same type of active material. Generally, EDLCs employ activated carbon (AC) as the active material, which is commonly derived from natural resources or biomass waste. AC is preferred due to its large surface area, tunable pore structure, low cost, abundant raw sources, and facile synthesis process [3], [4]. Pseudocapacitors exhibit higher energy storage capacity than EDLCs, whereas EDLCs possess superior cycle stability. Charge

storage in pseudocapacitors occurs through fast and reversible surface redox reactions [5]. Pseudocapacitors generally employ active materials such as metal oxides and conducting polymers. Meanwhile, hybrid supercapacitors are classified as asymmetric supercapacitors because the cathode and anode are composed of different active electrode materials [6].

MXene is an active electrode material for pseudocapacitors, classified as a two-dimensional (2D) transition metal carbide or nitride. MXene has a layered structure with higher electrical conductivity compared to metal oxides, enabling rapid charge transfer. The general formula of MXene is $M_{n+1}X_nT_x$, where M is a transition metal such as Ti, V, Nb, Cr, and Mo, while X is carbon (C) [7]. Among various MXenes, $Ti_3C_2T_x$ has been widely utilized in pseudocapacitor applications due to the high electrical conductivity (~10,000 Scm^{-1}) and remarkable specific capacitance exhibited under negative potential [8]. $Ti_3C_2T_x$ is synthesized by selectively etching the Al layer from Ti_3AlC_2 (MAX phase) using acidic solutions such as hydrofluoric acid (HF).

In a symmetric supercapacitor, MXene composited with polyindole in a 3:1 ratio delivers a specific capacitance of 226.5 Fg^{-1} at a current density of 2 Ag^{-1}, with a cyclic stability of 90.5% after 8000 cycles, which is higher than that of the asymmetric configuration of MXene and polyindole [9]. Similarly, a symmetric supercapacitor based on carbon and MXene exhibits 94% stability after 5000 cycles, with a capacitance of 250.6 Fg^{-1} at 1 Ag^{-1} [10]. On the other hand, in asymmetric supercapacitor applications, MXene/NiS as the anode and G/AC as the cathode demonstrate outstanding electrochemical performance, achieving a specific capacitance of 857.8 Fg^{-1}, an energy density of 17.688 Wh kg^{-1}, and a power density of 750 Wkg^{-1} [11]. In other previous studies, MXene used as the anode and AC as the cathode achieved a volumetric capacitance of 250 Fcm^{-3} with a cycling stability of 122% after 6,000 cycles [12]. The configuration and substrate employed also influence the electrochemical performance of the supercapacitor. MXene was used as the cathode and AC as the anode, both deposited on nickel foam, achieving a specific capacitance of 36.61 Fg^{-1} with 53.10% capacitance retention after 10,000 cycles [13]. In another configuration, MXene was employed as the anode and AC as the cathode on a titanium substrate, achieving an energy density of 34 $Whkg^{-1}$, a power density of 954 Wkg^{-1}, and 79% capacitance retention after 100,000 cycles [14].

MXene and AC have been widely used as active materials for symmetric and asymmetric supercapacitors. Previous research has explored the synthesis of activated carbon derived from a combination of cassava tubers and bamboo stems. Natural resources such as cassava and bamboo exhibit high productivity in Indonesia. AC cassava tubers-bamboo stems assembled into a symmetric supercapacitor exhibits a three-dimensional porous structure composed of micro-, meso-, and macropores, achieving a power density of up to 1086.12 Wkg^{-1} and a cycling stability of 90.8% after 5000 cycles [3]. To date, no study has comprehensively investigated the electrode configurations of MXene and AC cassava tubers-bamboo stems in symmetric and asymmetric arrangements. Therefore, the present study systematically investigates the influence of different electrode configurations of MXene and AC cassava tubers-bamboo stems under symmetric and asymmetric arrangements. Furthermore, this study aims to determine the role of the composition and configuration of MXene and AC cassava tubers-bamboo stems electrodes in improving the electrochemical performance of supercapacitors.

2. Methods

2.1 Synthesis of MXene

MXene was synthesized using the aluminum atomic layer etching method of Ti_3AlC_2 (MAX phase). In this process, 4 g of Ti_3AlC_2 were added to 80 mL of 49% hydrogen fluoride (HF) solution and stirred at 500 rpm for 24 h at room temperature. The resulting product was repeatedly washed with distilled water until a neutral pH was achieved, followed by drying in a vacuum oven at 80 °C for 24 h.

2.2 Synthesis of AC cassava tubers-bamboo stems

The cassava waste used in this study was derived from tubers, while the bamboo waste was obtained from the stems. The activated carbon synthesis followed the procedure reported in previous research [3]. Cassava tubers and bamboo stems were cut to a size of ± 5 cm, then dried in the sun for 12 h until completely dry. Each precursor was pre-carbonized at 400 °C for 2 h. Cassava tuber carbon and bamboo stem carbon were mixed with a mass ratio of 1:1. In the first step, 22.44 g of KOH were dissolved in 100 mL of deionized water and stirred at 500 rpm for 30 min at room temperature. Subsequently, 7.48 g of the mixed cassava tubers-bamboo stem carbon were added to the KOH solution

and stirred at 500 rpm for 24 h at room temperature. The obtained sample was washed with 1 M HCl, followed by repeated washing with distilled water until the pH became neutral. AC is dried at a temperature of 100°C for 24 h and then the final carbonization process is carried out at a temperature of 600°C for 1 h.

2.3 Preparation of thin-film electrode

The thin-film electrode slurry was prepared by mixing the active material, carbon black as a conductive additive, and LA133 binder in a ratio of 9:1:0.35. The asymmetric supercapacitor in this study employed MXene as the anode and AC cassava tubers-bamboo stems as the cathode active material. First, 0.35 g of LA133 was dissolved in 3 mL of deionized (DI) water and stirred at 200 rpm for 30 min at room temperature. Subsequently, 0.1 g of carbon black was added to the solution, followed by 0.9 g of the active material. The resulting mixture was stirred continuously for 24 h at room temperature to ensure uniform dispersion. The homogeneous MXene slurry was then coated onto a copper foil substrate, while the AC cassava tubers-bamboo stems slurry was coated onto another copper foil using a doctor blade with a wet film thickness of 20 μm. For the symmetric supercapacitor, the active material consisted of a mixture of MXene and cassava tubers-bamboo stems AC at a 1:1 ratio, which was deposited onto an aluminum foil substrate.

2.4 Microstructure characterization

The crystal structures of MAX, MXene and the AC derived from the combination of cassava tubers-bamboo stems was analyzed using X-ray diffraction (XRD, Pan Analytical, UK, Cu-Kα, λ = 0.15406 nm) over a 2θ range of 5° to 90°. The crystalline size (*D*, nm) and interlayer spacing (*d*, nm) of the XRD diffraction peaks from MAX and MXene samples were determined using Equation (1) and (2) [15].

$$D = (K \times \lambda_{hkl})/(\beta_{hkl} \times \cos\theta) \quad (1)$$

$$d = (n \times \lambda_{hkl})/(2 \times \sin\theta) \quad (2)$$

where K is the shape factor (0.94), λ_{hkl} is the X-ray wavelength (1.5406 Å), β_{hkl} is the full width at half maximum (FWHM) in radians, θ is the Bragg angle in radians, and n = 1 represents the order of reflection. The lattice parameters (a and c) of the MAX and MXene samples were determined using the interlayer spacing (d) equation for a hexagonal crystal structure as shown by Equation 3, where *hkl* are Miller indices [15].

$$d = \frac{1}{\sqrt{\frac{4}{3}\left(\frac{h^2 + hk + k^2}{a^2} + \frac{l^2}{c^2}\right)}} \quad (3)$$

The elemental composition and chemical states were examined using X-ray photoelectron spectroscopy (XPS, PHI5000 Versa Probe II, Japan). The surface morphology of MXene and the AC was characterized by scanning electron microscopy (SEM, FEI Inspect-S50). The specific surface area and pore structure were determined using Brunauer-Emmett-Teller (BET) analysis (Tristar II Plus 3020) with nitrogen (N_2) adsorption following degassing at 300°C.

2.5 Fabrication of supercapacitor and electrochemical characterization

The electrodes for the coin cell device were assembled using a cloth fiber separator and 1 M tetraethylammonium tetrafluoroborate (1 M Et_4NBF_4) dissolved in propylene carbonate (PC) as the electrolyte. Electrochemical measurements were performed using galvanostatic charge/discharge (GCD, Neware), cyclic voltammetry (CV), and electrochemical impedance spectroscopy (EIS) with an Autolab Metrohm PGSTAT302N. The electrochemical performance of the supercapacitor was evaluated based on the specific capacitance from the GCD ($C_{specific\ GCD}$, Fg^{-1}) as presented in Equations (4) [4], [16], [17].

$$C_{specific\ GCD} = 4\frac{I\Delta t}{m\Delta V} \quad (4)$$

I represent the applied current (A), Δt corresponds to the discharge duration (s), m indicates the mass of the active electrode material (g), $\int IdV$ indicates the integrated area under the CV curve, k is the scanrate (Vs^{-1}), and ΔV refers to the potential window (V). The energy density ($ED_{coincell}$, $Whkg^{-1}$) and power

density ($EP_{coincell}$, Wkg^{-1}) of the coin cell device were obtained from the GCD test results using equations (6) and (6).

$$ED_{coin\ cell\ GCD} = \frac{C_{specific\ GCD}\ V^2}{7.2} \tag{5}$$

$$EP_{coin\ cell\ GCD} = 3600 \frac{ED_{coin\ cell\ GCD}}{\Delta t} \tag{6}$$

3 Results and Discussion

3.1 Microstructure and morphology analysis

The XRD pattern of the MAX and MXene samples are presented in Figure 1. The effect of the etching process on the MAX phase is evident, as the MAX sample exhibits higher crystallinity compared to the MXene sample. According to the JCPDS PDF 00-722-1324 database, the diffraction peaks at approximately 2θ = 9° and 39° correspond to the (002) and (104) planes of Ti_3AlC_2 (MAX phase), respectively. After etching process, the (002) peak intensity decreases and the peak broadens, while the (104) peak disappears, which indicates the effective removal of Al layers during MXene formation.

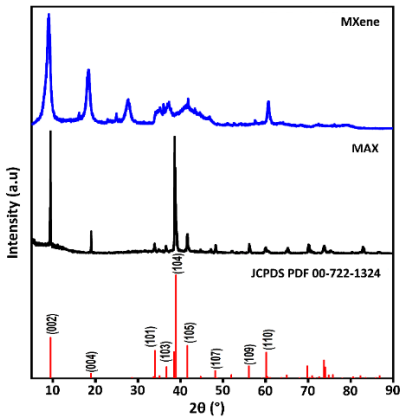

Figure 1. XRD Pattern of MAX and MXene.

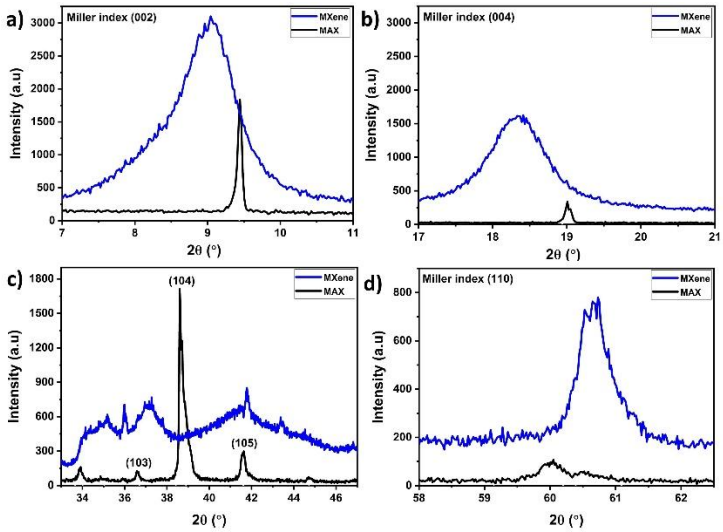

Figure 2. Enlarged XRD Patterns of MAX and MXene in the 2θ Range of (a) 7°- 11°, (b) 17°- 21°, (c) 33.5°- 46.5°, and (d) 58°- 63°.

Table 1. Crystalline Size (*D*), Interlayer Spacing (*d*), c-Lattice Parameter (*c*) of MAX and MXene Samples in Miller Index (002).

Sample	2θ (°)	β_{hkl} (°)	*D* (nm)	*d* (nm)	*c* (nm)
MAX	9.45	0.07	112.65	9.35	18.71
MXene	8.97	1.02	8.13	9.85	19.71

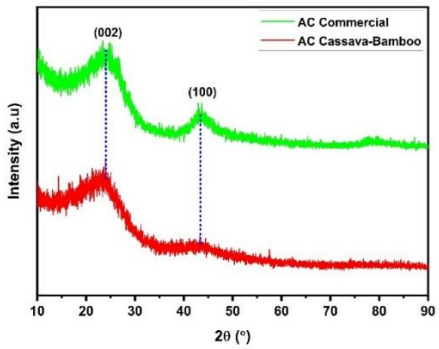

Figure 3. XRD Pattern of AC Cassava Tubers-Bamboo Stems and AC Commercial.

The MAX and MXene samples exhibit a hexagonal crystal structure with a space group of P63/mmc. The phase transformation in the MXene sample is evidenced by a broader shift in the diffraction peaks and the disappearance of certain peaks, as shown in Figure 2. The increase of the amorphous phase in the MXene samples also serves as evidence of phase change [18].

The crystallinity of the samples is indicated by the small FWHM value, as shown in Table 1. Table 1 shows the crystallite size and interlayer spacing of the MAX and MXene samples. The change in interlayer spacing indicate a phase or crystallographic transformation. As shown in Figure 2a, the use of HF as an etching agent to remove aluminum from the MAX phase not only broadens the (002) peak but also causes a peak shift from 9.447° to 8.968°. This shift in the (002) peak for the MXene sample affects its crystallite size. Based on Table 1, the MXene sample exhibits a smaller crystallite size (8.13 nm) compared to the MAX sample (112.65 nm). Furthermore, the MXene sample shows a larger interlayer spacing than the MAX phase. As shown in Figures 2a and 2b, the (002) and (004) peaks of MXene shift toward lower diffraction angles, suggesting an increase in the c-lattice parameter. The increase can be attributed to the adsorption of water molecules and the incorporation of functional groups between the MXene layers. The (002) peak shift also indicates structural expansion due to the removal of aluminum atoms [19]. The disappearance of the (104) peak shown in Figure 2c further confirms the successful formation of the MXene phase. Additionally, the appearance of the (110) peak at 2θ = 60° in the MXene sample, as illustrated in Figure 2d, represents the out-of-plane structure of MXene, validating the effective etching process using HF [20].

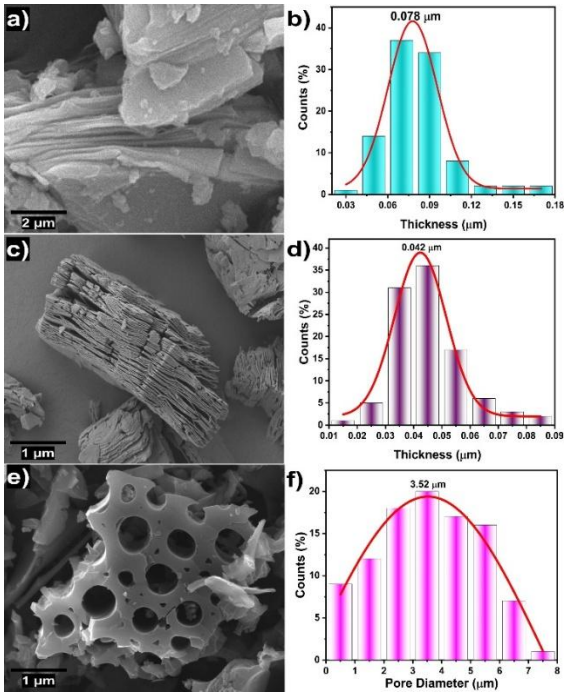

Figure 4. (a) SEM Morphology of MAX, (b) Thickness Distribution Histogram of MAX, (c) SEM Morphologies of MXene, (d) Thickness Distribution Histogram of MXene, (e) SEM morphologies of AC Cassava Tubers-Bamboo Stems, and (f) Thickness Distribution Histogram of AC Cassava Tubers-Bamboo Stems.

Based on Figure 3, the AC cassava tubers-bamboo stems and AC commercial exhibit two diffraction peaks corresponding to the (002) and (100) planes at 2θ values of 23.76° and 43.30°, respectively. The diffraction peaks indicate the formation of a graphitic structure during the synthesis and carbonization processes [21]. The (002) peak in activated carbon indicates an irregular and amorphous carbon structure, which has potential as an efficient electrode active material. The (100) peak represents the conductivity properties of activated carbon, which contribute to achieving superior electrochemical performance in supercapacitor devices. Acid washing followed by neutralization after the KOH activation process produced activated carbon without additional peaks in the XRD pattern, confirming the elimination of residual impurities in the sample.

Figure 4 presents the SEM morphologies of the MAX, MXene, and AC cassava tubers-bamboo stems. As shown in Figure 4a and 4b, the MAX sample shows a thick layered plate with a thickness of 0.078 µm. The MAX sample exhibits a thick plate-like structure with tightly stacked layers and few visible gaps, which result from the presence of aluminum atoms. After the HF etching process, the aluminum atoms are removed, leading to the exfoliation of the layers into thinner sheets and the formation of interlayer gaps, as shown in Figure 4c. Figure 4d presents the histogram of the thickness distribution of the MXene planar layers, which measures 0.042 µm, smaller compared to the MAX sample. Compared with the MAX phase, the planar MXene layers display reduced thickness and a more separated structure. In contrast, Figure 4e reveals that the AC cassava tubers-bamboo stems sample possesses a three-dimensional porous morphology. This structure is characterized by circular pores surrounded by smaller triangular pores, resembling a sunflower-like pattern, consistent with previous research [3]. Based on Figure 4f, the pore diameter distribution histogram shows that the average pore diameter of the AC cassava tubers-bamboo stems sample is 3.52 µm.

3.2 Electrochemical performances

The electrochemical performances of MXene and AC cassava tubers-bamboo stems-based coin cell supercapacitors is presented based on the results of GCD, CV, and EIS tests conducted using a 1M Et_4NBF_4/PC electrolyte.

Based on the GCD test results presented in Figure 5, the specific capacitance, energy density, and power density for each sample are shown in Table 2. The GCD analysis of electrode materials based on MXene and AC derived from cassava tubers–bamboo stems demonstrates that the optimal performance was achieved by the AC-MXene-Al Foil//AC-MXene-Cu Foil sample. The AC-MXene-Al Foil//AC-MXene-Cu Foil sample exhibited the highest specific capacitance, energy density, and power density, reaching 46.201 F g^{-1}, 5.770 Wh kg^{-1}, and 18.996 W kg^{-1}, respectively. As shown in Figure 5, the longer discharge time of the AC-MXene-Al Foil//AC-MXene-Cu Foil sample indicates higher charge storage capability, which corresponds to increased energy and power densities. The AC-MXene-Al Foil//AC-MXene-Cu Foil configuration consists of a 1:1 composite of MXene and AC cassava tubers–bamboo stems, assembled into a coin cell using different substrates.

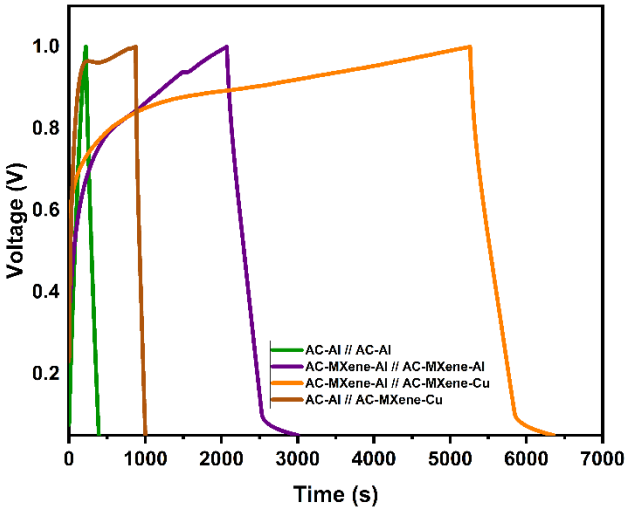

Figure 5. GCD Graph of Each Coincell Supercapacitor Sample.

Table 2. Specific Capacitance, Energy Density, and Power Density for Each Coin Cell Supercapbatteries from GCD at Current Density of 0.01 Ag^{-1}.

Types of Supercapacitors	Composition		Specific Capacitance (Fg^{-1})	Energy Density ($Whkg^{-1}$)	Power Density (Wkg^{-1})
	Cathode	Anode			
Symmetric	AC/CB/LA133/Al Foil	AC/CB/LA133/Al Foil	32.802	4.442	18.904
	AC/MXene/CB/LA133/Al Foil	AC/MXene/CB/LA133/Al Foil	39.506	4.925	18.948
Asymmetric	AC/MXene/CB/LA133/Al Foil	AC/MXene/CB/LA133/Cu Foil	46.201	5.770	18.996
	AC/CB/LA133/Al Foil	MXene/CB/LA133/Cu Foil	26.743	3.277	18.786

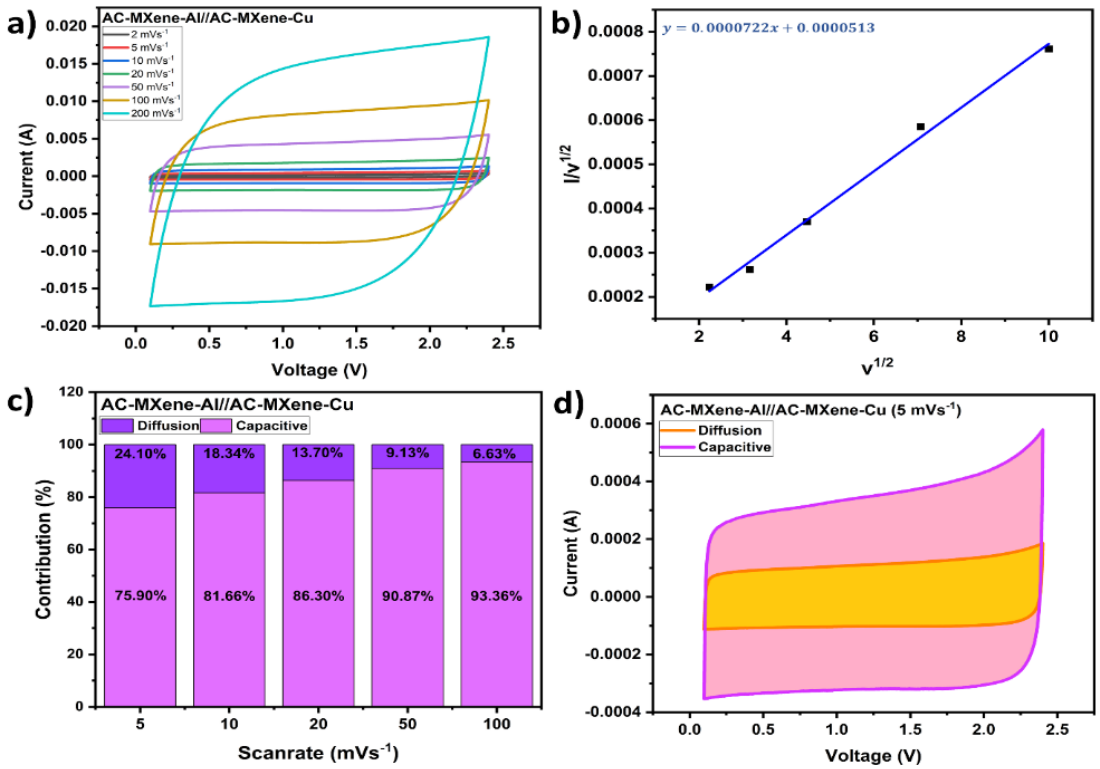

Figure 6. (a) CV Graph of Each Coincell Supercapacitor Sample, (b) the Plot of $I/v^{1/2}$ with $v^{1/2}$, (c, d) Analysis the Dunn Method.

The AC/MXene composite provides a combination of the capacitive properties of AC and the high electrical conductivity of MXene. AC supports ion transport and electrolyte infiltration due to its porous structure, while MXene's high conductivity enhances charge storage rate capability [22]. The use of two different substrates effectively improves electron transfer and ion transport, resulting in superior energy storage performance. Furthermore, Table 2 indicates that the lowest electrochemical performance was obtained from the asymmetric coin cell composed of AC/CB/LA133/Al Foil//MXene/CB/LA133/Cu Foil. These findings suggest that although asymmetric configurations can expand the voltage window, maintaining charge balance between the two electrodes remains a critical factor.

Based on Figure 6(a), the CV curves of the AC-MXene-Al Foil//AC-MXene-Cu Foil sample at various scan rates (2–200 mV s^{-1}) show the electrochemical behavior of the electrode system. The CV curves exhibit an approximately rectangular shape, indicating a dominant electric double-layer capacitance (EDLC) behavior. However, a slight distortion at higher potentials suggests the presence of pseudocapacitive contributions arising from surface redox reactions on MXene [23]. The analysis

using the Dunn method is presented in Figures 6(b–d). The Dunn method equation ($i/v^{0.5} = k_1 v^{0.5} + k_2$) results in a plot of $v^{0.5}$ versus $i/v^{0.5}$ exhibiting good linearity, as illustrated in Figure 6(b). Figure 6(c) shows that the capacitive contribution increases with increasing scan rate, while the diffusion contribution decreases from 24.10% to 6.63%. These findings suggest that at higher scan rates, charge storage is predominantly governed by surface capacitive mechanisms, attributed to the large active surface area of activated carbon and the high electrical conductivity of MXene. As shown in Figure 6(d), the current separation plot reveals a significantly larger capacitive area compared to the diffusion area, confirming that the energy storage process is primarily controlled by capacitive behavior [24].

4 Conclusion

The supercapacitor active material based on MXene and AC cassava tubers-bamboo stems exhibited excellent microstructural, morphological, and electrochemical characteristics. The etching process using HF successfully transformed the MAX phase (Ti_3AlC_2) into MXene ($Ti_3C_2T_x$), as confirmed by the disappearance of the (104) diffraction peak and the shift of the (002) peak toward a lower diffraction angle. This peak shift indicates an increased interlayer spacing due to the removal of aluminum atoms and the intercalation of functional groups and water molecules. According to the SEM characterization, MXene displays a larger interlayer distance and a reduction in crystallite size from 112.65 nm to 8.13 nm, confirming the successful formation of a two-dimensional MXene structure with high electrical conductivity. The AC cassava tubers-bamboo stems shows an amorphous graphitic structure with a three-dimensional pore network resembling a sunflower pattern, possessing an average pore diameter of 3.52 µm. This structure enhances the active surface area and facilitates efficient electrolyte ion transport. Electrochemical testing demonstrated that the AC-MXene-Al Foil//AC-MXene-Cu Foil configuration exhibited the best performance, delivering a specific capacitance of 46.201 Fg^{-1}, an energy density of 5.770 $Whkg^{-1}$, and a power density of 18.996 Wkg^{-1}. The longer discharge time indicates a higher charge storage capability. The Dunn method analysis revealed that the energy storage mechanism is predominantly governed by surface capacitive behavior, with the diffusion contribution decreasing from 24.10% to 6.63% as the scan rate increases. These findings highlight the great potential of the biomass-derived AC/MXene composite for the development of high-performance and environmentally friendly energy storage devices.

Acknowledgment

This research was funded by the 2024 National Competitive Grant from the Directorate of Research, Technology, and Community Service, Ministry of Higher Education, Research, and Technology, under the PTM-specific scheme by Universitas Negeri Malang.

References

[1] K. Liu *et al.*, "Flexible electrode materials for emerging electronics: materials, fabrication and applications," *J. Mater. Chem. A*, vol. 12, no. 32, pp. 20606–20637, 2024, doi: 10.1039/D4TA01960A.

[2] Z. Dong *et al.*, "A Survey of Battery–Supercapacitor Hybrid Energy Storage Systems: Concept, Topology, Control and Application," *Symmetry (Basel).*, vol. 14, no. 6, p. 1085, May 2022, doi: 10.3390/sym14061085.

[3] M. Diantoro *et al.*, "3D-porous activated carbon morphological modification of Manihot esculenta tuber and Bambusa blumeana stem for high-power density supercapacitor: Biomass waste to sustainable energy," *Carbon Resour. Convers.*, p. 100313, Mar. 2025, doi: 10.1016/j.crcon.2025.100313.

[4] H. Rustamaji *et al.*, "Synthesis of rubber seed shell-derived porous activated carbons for promising supercapacitor application," *Int. J. Renew. Energy Dev.*, vol. 14, no. 2, pp. 265–275, Mar. 2025, doi: 10.61435/ijred.2025.60869.

[5] R. Chen, M. Yu, R. P. Sahu, I. K. Puri, and I. Zhitomirsky, "The Development of Pseudocapacitor Electrodes and Devices with High Active Mass Loading," *Adv. Energy Mater.*, vol. 10, no. 20, May 2020, doi: 10.1002/aenm.201903848.

[6] N. Wu *et al.*, "Recent Advances of Asymmetric Supercapacitors," *Adv. Mater. Interfaces*, vol. 8, no. 1, Jan. 2021, doi: 10.1002/admi.202001710.

[7] K. Khan *et al.*, "Recent Advances in Non-Ti MXenes: Synthesis, Properties, and Novel Applications," *Adv. Sci.*, vol. 11, no. 36, Sep. 2024, doi: 10.1002/advs.202303998.
[8] L. Ma, T. Zhao, F. Xu, T. You, and X. Zhang, "A dual utilization strategy of lignosulfonate for MXene asymmetric supercapacitor with high area energy density," *Chem. Eng. J.*, vol. 405, p. 126694, Feb. 2021, doi: 10.1016/j.cej.2020.126694.
[9] S. De, C. K. Maity, S. Sahoo, and G. C. Nayak, "Polyindole Booster for Ti_3C_2T x MXene Based Symmetric and Asymmetric Supercapacitor Devices," *ACS Appl. Energy Mater.*, vol. 4, no. 4, pp. 3712–3723, Apr. 2021, doi: 10.1021/acsaem.1c00142.
[10] Z. Pan and X. Ji, "Facile synthesis of nitrogen and oxygen co-doped $C@Ti_3C_2$ MXene for high performance symmetric supercapacitors," *J. Power Sources*, vol. 439, p. 227068, Nov. 2019, doi: 10.1016/j.jpowsour.2019.227068.
[11] H. Liu *et al.*, "A facile method for synthesizing NiS nanoflower grown on MXene (Ti_3C_2Tx) as positive electrodes for 'supercapattery,'" *Electrochim. Acta*, vol. 353, p. 136526, Sep. 2020, doi: 10.1016/j.electacta.2020.136526.
[12] Y. Tian, C. Yang, Y. Tang, Y. Luo, X. Lou, and W. Que, "Ti_3C_2T //AC dual-ions hybrid aqueous supercapacitors with high volumetric energy density," *Chem. Eng. J.*, vol. 393, p. 124790, Aug. 2020, doi: 10.1016/j.cej.2020.124790.
[13] V. Thirumal, P. Rajkumar, B. Babu, J.-H. Kim, and K. Yoo, "Performance of asymmetric hybrid supercapacitor device based on antimony-titanium carbide MXene composite," *J. Alloys Compd.*, vol. 982, p. 173598, Apr. 2024, doi: 10.1016/j.jallcom.2024.173598.
[14] W. Chen *et al.*, "V_2CT_x MXene as novel anode for aqueous asymmetric supercapacitor with superb durability in $ZnSO_4$ electrolyte," *J. Colloid Interface Sci.*, vol. 626, pp. 59–67, Nov. 2022, doi: 10.1016/j.jcis.2022.06.142.
[15] S. Rafiq *et al.*, "Novel room-temperature ferromagnetism in Gd-doped 2-dimensional Ti3C2Tx MXene semiconductor for spintronics," *J. Magn. Magn. Mater.*, vol. 497, p. 165954, Mar. 2020, doi: 10.1016/j.jmmm.2019.165954.
[16] C. R. Babu, A. V. Avani, T. S. Xavier, M. Tomy, S. Shaji, and E. I. Anila, "Symmetric supercapacitor based on Co3O4 nanoparticles with an improved specific capacitance and energy density," *J. Energy Storage*, vol. 80, p. 110382, Mar. 2024, doi: 10.1016/j.est.2023.110382.
[17] B. J. Choudhury, H. H. Muigai, P. Kalita, and V. S. Moholkar, "Biomass blend derived porous carbon for aqueous supercapacitors with commercial-level mass loadings and enhanced energy density in redox-active electrolyte," *Appl. Surf. Sci.*, vol. 601, p. 154202, Nov. 2022, doi: 10.1016/j.apsusc.2022.154202.
[18] Y. Wen *et al.*, "Nitrogen-doped Ti3C2T x MXene electrodes for high-performance supercapacitors," *Nano Energy*, vol. 38, pp. 368–376, Aug. 2017, doi: 10.1016/j.nanoen.2017.06.009.
[19] H. Zhang *et al.*, "Gradient-Layered MXene/Hollow Lignin Nanospheres Architecture Design for Flexible and Stretchable Supercapacitors," *Nano-Micro Lett.*, vol. 17, no. 1, p. 43, Dec. 2025, doi: 10.1007/s40820-024-01512-3.
[20] L. Pradhan *et al.*, "Supercapacitor properties of partially oxidised-MXene quantum dots/graphene hybrids: Fabrication of flexible/wearable micro-supercapacitor devices," *Chem. Eng. J.*, vol. 497, p. 154587, Oct. 2024, doi: 10.1016/j.cej.2024.154587.
[21] P. Merin, P. Jimmy Joy, M. N. Muralidharan, E. Veena Gopalan, and A. Seema, "Biomass-Derived Activated Carbon for High-Performance Supercapacitor Electrode Applications," *Chem. Eng. Technol.*, vol. 44, no. 5, pp. 844–851, May 2021, doi: 10.1002/ceat.202000450.
[22] L. Yu *et al.*, "MXene-Bonded Activated Carbon as a Flexible Electrode for High-Performance Supercapacitors," *ACS Energy Lett.*, vol. 3, no. 7, pp. 1597–1603, Jul. 2018, doi: 10.1021/acsenergylett.8b00718.
[23] Z. He *et al.*, "Pseudocapacitance of Bimetallic Solid-Solution MXene for Supercapacitors with Enhanced Electrochemical Energy Storage," *Adv. Funct. Mater.*, vol. 33, no. 52, Dec. 2023, doi: 10.1002/adfm.202305251.
[24] S. Myeong, S. Ha, C. Lim, C. G. Min, and Y.-S. Lee, "Effect of fluorine functional groups introduced into activated carbon aerogel by carbon tetrafluoride plasmas in supercapacitors," *Carbon Lett.*, vol. 34, no. 1, pp. 65–74, Jan. 2024, doi: 10.1007/s42823-023-00668-z.